

## Invited Lecture An Introduction to Cavitation Fundamentals

Christopher E. Brennen  
California Institute of Technology, Pasadena, California, USA  
[brennen@caltech.edu](mailto:brennen@caltech.edu)

### ABSTRACT

In this opening lecture I will summarize some of the fundamentals of cavitation in the hope that this will allow attendees greater insight into the more advanced lectures which follow. Whether your primary interest is in the turbomachinery field or in the biological and bioengineering contexts in which cavitation is important these fundamentals are important in understanding the observed phenomena.

### NOMENCLATURE

$A_0$	Initial radius of the cloud of bubbles.
$A_N$	Nuclei capture streamtube area
$C_{PMIN}$	Minimum pressure coefficient in the flow
$f$	Frequency
$G(f)$	Spectral density function
$I$	Acoustic impulse
$I^*$	Dimensionless acoustic impulse
$l$	Reference length in the flow
$k$	Polytropic index
$N$	Nuclei concentration
$n^*$	Event rate
$p_a$	Radiated acoustic pressure
$p_s$	Acoustic pressure
$p_B$	Bubble pressure
$p_{oo}$	Reference pressure
$p_v$	Vapor pressure
$r$	Radial Coordinate
$R$	Bubble radius
$R_E$	Equilibrium radius of the bubbles
$R_H$	Headform radius
$R_0$	Initial radius of the bubbles
$R_m$	Maximum bubble radius
$R_N$	Nuclei radius
$R$	Distance from source
$S$	Surface tension
$t$	Time
$T_{oo}$	Reference temperature
$U_{oo}$	Reference velocity
$V$	Bubble volume
$T_{oo}$	Reference temperature
$\alpha_0$	Initial void fraction in the cloud.
$\beta$	Interaction parameter, $\propto A^2/R^2$ Also a coefficient in section 7

$\nu_L$	Liquid kinematic viscosity
$\rho_L$	Liquid density
$\sigma$	Cavitation number
$\sigma_i$	Cavitation inception number
$\omega_N$	Bubble natural frequency
$\omega_n$	Cloud natural frequencies
$\omega$	Radian frequency

### 1. INTRODUCTION

We begin where cavitation begins namely with the tiny nuclei which grow into observable cavitation bubbles for they hold the key to some of the complications in dealing with the phenomena. We then follow the growth and collapse of cavitation bubbles or other structures as they experience a low pressure episode followed by a pressure recovery. In doing so we will survey the various forms that the bubbles may take as well as phenomena they exhibit.

### 2. NUCLEATION

When a pure liquid is subjected to a pressure below its vapor pressure (at a given, uniform temperature) it is said to be *under tension*. If there is no vapor present, that state of tension can be stable and, like a solid, a pure liquid can sustain very large negative pressures without rupturing and forming vapor voids. This is not as surprising as it may seem when one considers that a liquid is very similar to a solid in terms of its density and intermolecular forces. Indeed the theoretical tension which a pure liquid (or solid) can sustain is of the order of  $3 \times 10^4$  to  $3 \times 10^5$  atmospheres [1]. Of course, in practice, pure solids cannot reach this level of tension and they yield at values about 100 times less because of stress concentrations and other imperfections within their structure. Liquids are similar except that the weaknesses that lower the achievable tension can take various different forms. One of these forms of weakness is the chance formation of small temporary gaps between molecules caused by random thermal motions of the molecules. The process of vapor bubble formation by this mechanism is called *homogeneous nucleation* and the corresponding limiting tension can be predicted by kinetic theory. Another potential weaknesses can

occur at the interface between the liquid and a solid in contact with the liquid. This is termed *heterogeneous nucleation*. Sometimes the solid surface may be that of the containing vessel or it may be a small suspended particle. Thirdly, a liquid can contain very small gas bubbles (microbubbles) which are stabilized by surface tension effects (supplemented sometimes by contaminant molecules) but which grow into macroscopic vapor bubbles under a sufficiently large tension. A fourth type of weakness is that caused by radiation from the outside. A collision between a high energy cosmic particle and a molecule of the liquid can deposit sufficient energy to initiate nucleation when it would otherwise have little chance of occurring. Such, of course, is the principal of the bubble chamber.

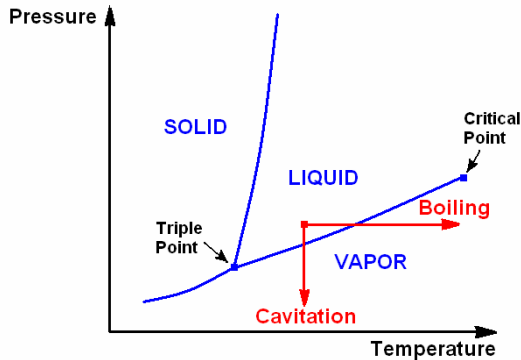


Figure 1. Phase diagram for a simple substance like water where the blue line between the triple point and the critical point is the saturated vapor/liquid line.

Each of these types of weakness will have a level of tension at which they will cause rupture of the liquid and the subsequent formation of vapor bubbles. The weakness that will first cause rupture will be that which requires the lowest tension. However, the relative tensions of each weakness will depend on the specific liquid, the specific thermodynamic state (pressure and temperature) and the specifics of the microbubbles and/or nucleation sites at the containing boundaries. There are certainly liquids which manifest homogeneous nucleation because the tension at which it occurs is smaller than that required to grow the microbubbles present in the liquid. However, this review will confine itself to the case of water (or aqueous solutions) at normal temperatures and pressures and it transpires that, in these circumstances, the tensions needed for homogeneous nucleation are much larger than those needed to grow the naturally occurring microbubbles. Consequently the dominant weaknesses are micron-sized bubbles (microbubbles) of contaminant gas, which could be present in crevices within the solid boundary or within suspended particles or could simply be freely suspended within the liquid. In water, microbubbles of air seem to persist almost indefinitely and are almost impossible to remove completely. They resist being dissolved completely, perhaps because of contamination of the interface.

We use the term *boiling* to refer to a process in which we change the thermodynamic state of a liquid by heating it at relatively constant pressure as shown by the horizontal arrow in figure 1. On the other hand the formation of bubbles resulting from depressurization at relatively constant temperature (the vertical arrow) is called *cavitation* (Note that the tension would be the vertical distance below the saturated vapour/liquid line at which cavitation occurs). Thermodynamically boiling and cavitation are identical for the path taken in crossing the saturated vapor/line line is of little consequence.

However, there are practical differences caused by the fact that while it is feasible to uniformly change the pressure throughout a large volume of liquid, it is very difficult to uniformly change the temperature. Thus boiling normally involves heating the liquid at a boundary and therefore the nucleation sites which are first activated are those at that boundary since the temperature is greatest there. On the other hand cavitation usually occurs in the body of a liquid. Consequently the most vulnerable nucleation sites in most cavitation processes in water are either microbubbles or solid particles containing microbubbles in crevices. Both are termed cavitation nuclei and are the nucleation sites for most aqueous cavitation phenomena. Many studies focus on methods for measuring these nuclei and on the effects that these nuclei have on the observed cavitation phenomena. Typical measurements of cavitation nuclei in water tunnels and in the ocean are shown in Figure 2. Note that most of the relevant nuclei

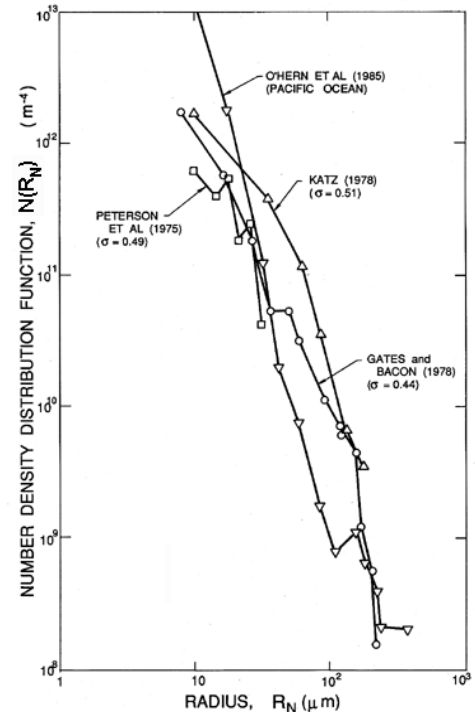


Figure 2. Cavitation nuclei number density distribution functions measured by holography in three different water tunnels (Peterson *et al.* [2], Gates and Bacon [3], Katz [4]) at the cavitation numbers,  $\sigma$ , as shown) and in the ocean off Los Angeles, Calif. (O'Hern *et al.* [5]).

range from about 5 $\mu\text{m}$  to 100 $\mu\text{m}$  in size. Smaller bubbles are stabilized by surface tension while the population of larger bubbles is very small since they tend to rise up and out of the liquid.

In most conventional engineering contexts, the prediction and control of nucleation sites is very uncertain even when dealing with a simple liquid like water. In other fluids such as cryogenic liquids or in complex biological substances, there is a much greater dearth of information.

### 3. CAVITATION INCEPTION

For cavitation in flowing systems it is conventional to characterize how close the pressure in the liquid flow is to the vapor pressure (and therefore the potential for cavitation) by means of the cavitation number,  $\sigma$ , defined as  $\sigma = 2(p_{\infty} - p_v)/\rho_L U_{\infty}^2$  where  $U_{\infty}$ ,  $p_{\infty}$  and  $T_{\infty}$  are respectively a reference velocity, pressure and temperature in the flow (usually upstream quantities),  $\rho_L$  is the liquid density and  $p_v(T_{\infty})$  is the saturated vapor pressure.

In a particular flow as  $\sigma$  is reduced, cavitation will first be observed to occur at some particular value of  $\sigma$  called the incipient cavitation number and denoted by  $\sigma_i$ . Further reduction in  $\sigma$  below  $\sigma_i$  would cause an increase in the number and size of the vapor bubbles. Suppose that prior to cavitation inception, the magnitude of the lowest pressure in the single phase flow is given by the minimum value of the coefficient of pressure,  $C_{pmin}$ . Note that  $C_{pmin}$  is a *negative* number and that its value could be estimated from either experiments or calculations of the single phase flow. Then, if cavitation inception were to occur when the minimum pressure reaches the vapor pressure it would follow that the value of the critical inception number,  $\sigma_i$ , would be simply given by

$$\sigma_i = -C_{pmin}.$$

Unfortunately, many factors can cause the actual values of  $\sigma_i$  to depart radically from  $-C_{pmin}$  and much research has been conducted to explore these departures because of the importance of determining  $\sigma_i$  accurately. Among the important factors are

- the ability of the liquid to sustain a tension so that bubbles do not grow to observable size until the pressure falls a finite amount below the vapor pressure. The magnitude of this tension is a function of the nuclei present in the liquid.
- the fact that cavitation nuclei require a finite residence time in which to grow to observable size.
- the fact that measurements or calculations usually yield a minimum coefficient of pressure that is a time-averaged value. On the other hand many of the flows with which one must deal in practice are turbulent and, therefore, nuclei in the middle of turbulent eddies may experience pressures below the vapor pressure even when

the mean pressure is greater than the vapor pressure.

Moreover, since water tunnel experiments designed to measure  $\sigma_i$  are often carried out at considerably reduced scale, it is also critical to know how to scale up these effects to accurately anticipate inception at the full scale.

A detailed examination of these effects is beyond the scope of this presentation and the reader is referred to Knapp, Daily and Hammitt [6], Acosta and Parkin [7], Arakeri [8] and Brennen [9] for further discussion.

### 4. BUBBLE GROWTH

Once initiated the growth and collapse of a bubble containing gas and vapor in reduced pressure surroundings will be governed by the Rayleigh-Plesset equation or variations of it. This connects the instantaneous bubble radius,  $R(t)$ , to the prevailing pressure,  $p_{\infty}(t)$ , far from the bubble:

$$\frac{p_B(t) - p_{\infty}(t)}{\rho_L} = R \frac{d^2 R}{dt^2} + \frac{3}{2} \left( \frac{dR}{dt} \right)^2 + \frac{4\nu_L}{R} \frac{dR}{dt} + \frac{2S}{\rho_L R}$$

where  $\nu_L$  is the liquid kinematic viscosity and  $S$  is the surface tension. A number of assumptions were made in deriving this equation including bubble spherical symmetry and that the thermal effects discussed later are negligible. Clearly the Rayleigh-Plesset equation is quite non-linear and solutions of it display features caused by that non-linearity. While bubble growth tends to be a fairly steady (though often explosive) as sketched in Figure 3, collapse tends to be catastrophic and to terminate in a minute bubble in which the non-condensable gas is so highly compressed that the adiabatic heating is substantial (see below).

It will be useful to develop an estimate of the maximum size to which a cavitation bubble grows during its trajectory through a region where the pressure is below the vapor pressure. In a typical external flow around a body characterized by the dimension,  $\ell$ , it follows from the Rayleigh-Plesset equation that the rate of growth is roughly given by

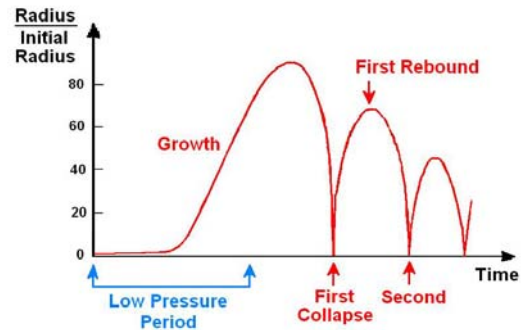


Figure 3. Typical bubble radius response to an episode of low pressure according to the Rayleigh-Plesset equation.

$$\frac{dR}{dt} = U_{\infty}(-\sigma - C_{pmin})^{\frac{1}{2}}$$

It should be emphasized this equation implies explosive growth of the bubble, in which the volume is increasing like  $t^3$ .

To obtain an estimate of the maximum size to which the cavitation bubble grows,  $R_m$ , a measure of the time it spends below vapor pressure is needed. Assuming that the pressure distribution near the minimum pressure point is roughly parabolic [9] the length of the region below vapor pressure will be proportional to

$$\ell(-\sigma - C_{pmin})^{\frac{1}{2}}$$

and therefore the time spent in that region will be the same quantity divided by  $U_{\infty}$ . The result is that an estimate of maximum size,  $R_m$ , is

$$R_m \approx 2\ell(-\sigma - C_{pmin})$$

where the factor 2 comes from the more detailed analysis of Brennen [9]. Note that, whatever their initial size, all activated nuclei grow to roughly the same maximum size because both the asymptotic growth rate and the time available for growth are essentially independent of the size of the original nucleus. For this reason all of the bubbles in a bubbly cavitating flow grow to roughly the same size independent of the size of the initial nucleus [9].

## 5. THERMAL EFFECTS

The above discussion (and the quoted version of the Rayleigh-Plesset equation) assumed that no significant temperature differences were generated in the liquid during growth. This is only the case in some liquids at lower temperatures (for example, water at normal temperatures). In other liquids or at higher temperatures, temperature differences develop between the bulk of the liquid and the vapor/liquid interface which substantially alter and inhibit the growth rate. This is termed the *thermal effect* or *thermodynamic benefit* for, by inhibiting growth, it reduces the deleterious effects of cavitation. The primary effect is caused by the major increase in the vapor density with increasing temperature. At low temperatures, the low vapor density means that only a small mass of liquid needs to be vaporized in order to allow bubble growth and this results in only minor cooling of the interface and therefore only a minor depression in the bubble temperature, pressure and growth rate. The effects become much greater at higher liquid temperatures. In water significant thermal effects do not usually begin until the temperature exceeds about 60°C. In cryogenic liquids they can be very important.

## 6. BUBBLE NATURAL FREQUENCIES

One derivation from the above Rayleigh-Plesset equation which is useful to mention is the natural frequency of oscillation of a single bubble in an infinite liquid domain. By examining the relation between small amplitude pressure perturbations and the linearized oscillations in the bubble radius that those pressure

fluctuations produce, it is readily shown that the bubble has a natural frequency,  $\omega_N$ , given by

$$\omega_N = \left[ \frac{1}{\rho_L R_E^2} \left\{ 3k(\bar{p}_{\infty} - p_V) + 2(3k - 1) \frac{S}{R_E} \right\} \right]^{\frac{1}{2}}$$

where  $R_E$  is the mean or equilibrium radius of the bubble,  $(p_{\infty} - p_V)$  is the mean liquid pressure minus vapor pressure and  $k$  is a polytropic index for the non-condensable gas in the bubble. This yields natural frequencies typified by those for water in Figure 4. Notice that bubbles in the range 10 $\mu$ m to 100 $\mu$ m have natural frequencies in the range 10 to 100kHz.

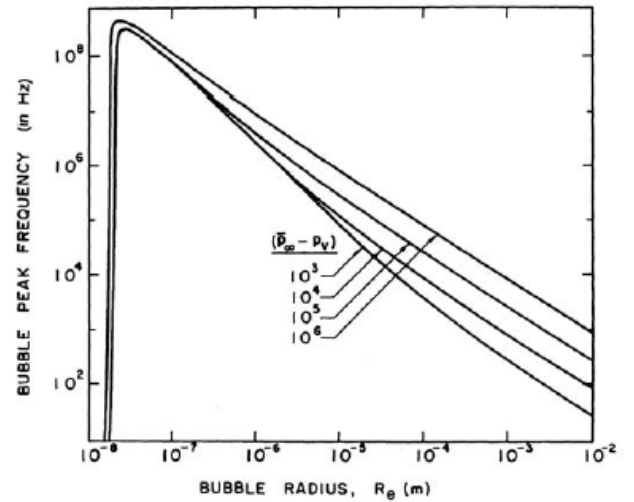


Figure 4. Bubble resonant frequencies in water at 300°K as a function of the radius of the bubble for various pressure levels,  $(p_{\infty} - p_V)$ .

## 7. CAVITATION BUBBLE COLLAPSE

One of the important non-linear effects in bubble dynamics is that vapor or cavitation bubble collapse in the absence of thermal effects can lead to very large interface velocities and very high localized pressures. This violence has important technological consequences for it can damage nearby solid surfaces in critical ways. Here we briefly review the fundamental processes associated with the phenomena of cavitation bubble collapse. For further details, the reader is referred to more specialized texts such as Knapp *et al.* [10], Young [11] or Brennen [9].

Integration of the Rayleigh-Plesset equation allows approximate evaluation of the magnitudes of the velocities, pressures, and temperatures generated by cavitation bubble collapse under a number of assumptions including that the bubble remains spherical. Though it will be later described that collapsing bubbles do not remain spherical, the spherical analysis provides a useful starting point. When a cavitation bubble grows from a small nucleus to many times its original size, the collapse will begin at a maximum radius,  $R_m$ , with a



partial pressure of gas,  $p_{Gm}$ , that is very small indeed. In a typical cavitating flow  $R_m$  is of the order of 100 times the original nuclei size,  $R_o$ . Consequently, if the original partial pressure of gas in the nucleus was about 1bar the value of  $p_{Gm}$  at the start of collapse would be about  $10^{-6}$ bar. Using a typical value of the liquid pressure decrease causing cavitation, it can be demonstrated [9] that the maximum bubble pressure generated in the first collapse would be about  $10^{10}$  bar and the maximum temperature would be  $4 \times 10^4$  times the ambient temperature! Many factors, including the diffusion of gas from the liquid into the bubble and the effect of liquid compressibility, mitigate this result. Nevertheless, the calculation illustrates the potential for the generation of high pressures and temperatures during collapse and the potential for the generation of shock waves and noise. Early work on collapse by Herring [12], Gilmore [13]] and others focused on the inclusion of liquid compressibility in order to learn more about the production of shock waves in the liquid generated by bubble collapse. Modifications to the Rayleigh-Plesset equation that would allow for liquid compressibility were developed and these are reviewed by Prosperetti and Lezzi [12]. A commonly used variant is that proposed by Keller and Kolodner [13].

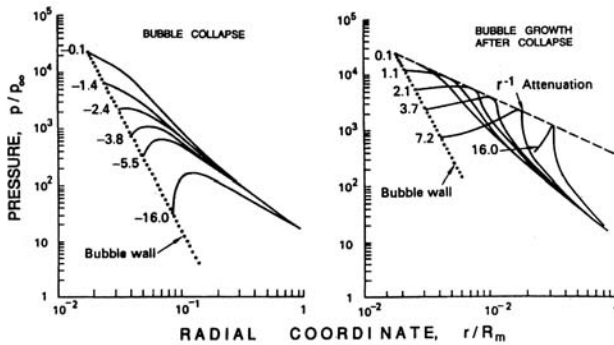


Figure 5. Typical results of Hickling and Plesset [14] for the pressure distributions in the liquid before collapse (left) and after collapse (right) (without viscosity or surface tension). The values attached to each curve are proportional to the time before or after the minimum size

However, as long as there is some non-condensable gas present in the bubble to decelerate the collapse, the primary importance of liquid compressibility is not the effect it has on the bubble dynamics (which is slight) but the role it plays in the formation of shock waves during the rebounding phase that follows collapse. Hickling and Plesset [14] were the first to make use of numerical solutions of the compressible flow equations to explore the formation of pressure waves or shocks during the rebounding phase that follows collapse. Figure 5 presents an example of their results for the pressure distributions in the liquid before (left) and after (right) the moment of minimum size. The graph on the right clearly shows the propagation of a pressure pulse or shock away from the bubble following the minimum size. As indicated in that figure, Hickling and Plesset concluded

that the pressure pulse exhibits approximately geometric attenuation (like  $r^{-1}$ ) as it propagates away from the bubble. Other numerical calculations have since been carried out by Ivany and Hammitt [15], Tomita and Shima [16], and Fujikawa and Akamatsu [17], among others.

Even if thermal effects are negligible for most of the collapse phase, they play a very important role in the final stage of collapse when the bubble contents are highly compressed by the inertia of the in-rushing liquid. The pressures and temperatures that are predicted to occur in the gas within the bubble during spherical collapse are very high indeed. Since the elapsed times are so small (of the order of microseconds), it would seem a reasonable approximation to assume that the noncondensable gas in the bubble behaves adiabatically. Typical of the adiabatic calculations is the work of Tomita and Shima [16] who obtained maximum gas temperatures as high as  $8800^\circ\text{K}$  in the bubble center. Such elevated temperatures and pressures only exist for a fraction of a microsecond but they can produce remarkable effects such as sonoluminescence, flashes of light during bubble collapse.

All of the above analyses assume spherical symmetry. We will now focus attention on the stability of shape of a collapsing bubble before continuing discussion of the origins of cavitation damage.

## 8. SHAPE DISTORTION DURING BUBBLE COLLAPSE

Like any other accelerating liquid/gas interface, the surface of a bubble is susceptible to Rayleigh-Taylor instability [18,19]. As expected a bubble is most unstable to non-spherical perturbations when it experiences the large, positive values of  $d^2R/dt^2$  that occur during the last stage of collapse. This has several different consequences. When the bubble surroundings are strongly asymmetrical (for example the bubble is close to a solid wall or a free surface) the dominant perturbation that develops is a re-entrant jet. Of particular interest for cavitation damage is the fact that a nearby solid boundary can cause a re-entrant microjet directed toward that boundary. The surface of the bubble furthest from the wall accelerates inward more rapidly than the side close to the wall and this results in a high-speed re-entrant microjet that penetrates the bubble and can achieve very high speeds. Such microjets were first observed experimentally by Naude and Ellis [20] and Benjamin and Ellis [21]. The series of photographs shown in figure 6 represent a good example of the experimental observations of a developing re-entrant jet. Figure 7 presents a comparison between the re-entrant jet development in a bubble collapsing near a solid wall as observed by Lauterborn and Bolle [23] and as computed by Plesset and Chapman [24].

Note also that depth charges rely for their destructive power on a re-entrant jet directed toward the submarine upon the collapse of the explosively generated bubble.

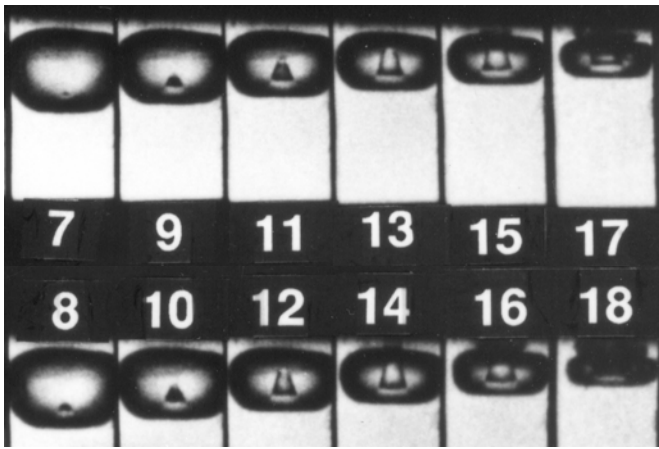


Figure 6. Series of photographs showing the development of the microjet in a bubble collapsing very close to a solid wall (at top of frame). The interval between the numbered frames is  $2\mu\text{s}$  and the frame width is 1.4mm [22].

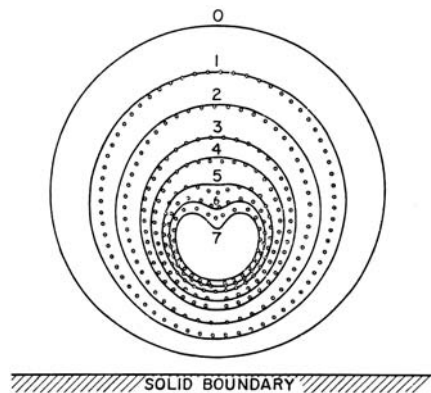


Figure 7. The collapse of a cavitation bubble close to a solid boundary in a quiescent liquid. The theoretical shapes of Plesset and Chapman [24] (solid lines) are compared with the experimental observations of Lauterborn and Bolle [23] (points) [25].

Other strong asymmetries can also cause the formation of a re-entrant jet. A bubble collapsing near a free surface produces a re-entrant jet directed away from the free surface [26]. Indeed, there exists a critical flexibility for a nearby surface that separates the circumstances in which the re-entrant jet is directed away from rather than toward the surface. Gibson and Blake [27] demonstrated this experimentally and analytically and suggested flexible coatings or liners as a means of avoiding cavitation damage. Another possible asymmetry is the proximity of other, neighboring bubbles in a finite cloud of bubbles. Chahine and Duraiswami [28] showed that the bubbles on the outer edge of such a cloud will tend to develop jets directed toward the center of the cloud.



Figure 8. Photographs of an ether bubble in glycerine before (left) and after (center and right) a collapse and rebound, both bubbles being about 5-6mm across [29].

When there is no strong asymmetry, the analysis of the Rayleigh-Taylor instability shows that the most unstable mode of shape distortion can be a much higher-order mode. These higher order modes can dominate when a vapor bubble collapses far from boundaries. Thus observations of collapsing cavitation bubbles, while they may show a single vapor/gas volume prior to collapse, just after minimum size the bubble appears as a cloud of much smaller bubbles. An example of this is shown in figure 8.

Brennen [9] shows how the most unstable mode depends on two parameters representing the effects of surface tension and non-condensable gas in the bubble. That most unstable mode number was later used in one of several analyses seeking to predict the number of fission fragments produced during collapse of a cavitating bubble [30].

## 9. CAVITATION DAMAGE

Perhaps the most ubiquitous engineering problem caused by cavitation is the material damage that cavitation bubbles can cause when they collapse in the vicinity of a solid surface. Consequently, this subject has been studied quite intensively for many years (see, for example, ASTM [31], Thiruvengadam [32, 33], Knapp, Daily, and Hammitt [6]). The problem is a difficult one because it involves complicated unsteady flow phenomena combined with the reaction of the particular material of which the solid surface is made. Though there exist many empirical rules designed to help the engineer evaluate the potential cavitation damage rate in a given application, there remain a number of basic questions regarding the fundamental mechanisms involved. Cavitation bubble collapse is a violent process that generates highly localized, large-amplitude shock waves and microjets. When this collapse occurs close to a solid surface, these intense disturbances generate highly localized and transient surface stresses. With softer material, individual pits caused by a single bubble collapse are often observed. But with the harder materials used in most applications it is the repetition of the loading due to repeated collapses that causes local surface fatigue failure and the subsequent detachment of pieces of material. Thus cavitation damage to metals usually has the crystalline appearance of fatigue failure. The damaged runner and pump impeller in figures 9 and 10 are typical examples.

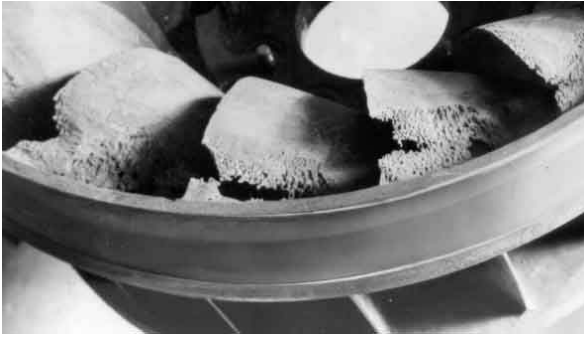


Figure 9. Major cavitation damage to the blades at the discharge from a Francis turbine.



Figure 10. Photograph of localized cavitation damage on the blade of a mixed flow pump impeller made from an aluminum-based alloy.

The issue of whether cavitation damage is caused by microjets or by shock waves generated when the remnant cloud of bubble reaches its minimum volume (or by both) has been debated for many years. In the 1940s and 1950s the focus was on the shock waves generated by spherical bubble collapse. When the phenomenon of the microjet was first observed, the focus shifted to studies of the impulsive pressures generated by microjets. First Shima *et al.* [34] used high speed Schlieren photography to show that a spherical shock wave was indeed generated by the remnant cloud at the instant of minimum volume. About the same time, Fujikawa and Akamatsu [17] used a photoelastic material so that they could simultaneously observe the stresses in the solid and measure the acoustic pulses and were able to confirm that the impulsive stresses in the material were initiated at the same moment as the acoustic pulse. They also concluded that this corresponded to the instant of minimum volume and that the waves were not produced by the microjet. Later, however, Kimoto [35] observed stress pulses that resulted both from microjet impingement and from the remnant cloud collapse shock.

The microjet phenomenon in a quiescent fluid has been extensively studied analytically as well as experimentally. Plesset and Chapman [24] numerically calculated the distortion of an initially spherical bubble as it collapsed close to a solid boundary and, as figure 7 demonstrates, their profiles are in good agreement with

the experimental observations of Lauterborn and Bolle [23].

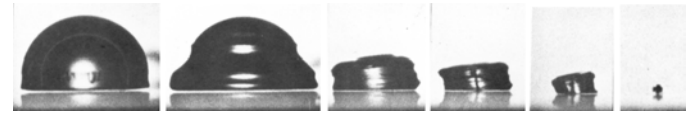


Figure 11. Series of photographs of a hemispherical bubble collapsing against a wall showing the *pancaking* mode of collapse [21].

It must also be noted that there are many circumstances in which it is difficult to discern a microjet. Some modes of bubble collapse near a wall involve a *pancaking* mode exemplified by the photographs in figure 11 and in which no microjet is easily recognized.

Finally, it is important to emphasize that virtually all of the observations described above pertain to bubble collapse in an otherwise quiescent fluid. A bubble that grows and collapses in a flow is subject to other deformations that can significantly alter its collapse dynamics, modify or eliminate the microjet and alter the noise and damage potential of the collapse process. In the next section some of these flow deformations will be illustrated.

## 10. CAVITATION BUBBLES IN FLOWS

We end our brief survey of the dynamics of cavitating bubbles with some experimental observations of single bubbles (single cavitation *events*) in real flows for these reveal the complexity of the micro-fluid-mechanics of individual bubbles. The focus here is on individual events springing from a single nucleus. The interactions between bubbles at higher nuclei concentrations will be discussed later.

Pioneering observations of individual cavitation events were made by Knapp and his associates at the California Institute of Technology in the 1940s (see, for example, Knapp and Hollander [36]) using high-speed movie cameras capable of 20,000 frames per second. Shortly thereafter Plesset [37], Parkin [38], and others began to model these observations of the growth and collapse of traveling cavitation bubbles using modifications of Rayleigh's original equation of motion for a spherical bubble. However, observations of real flows demonstrate that even single cavitation bubbles are often highly distorted by the pressure gradients in the flow.

Ceccio and Brennen [39] and Kuhn de Chizelle *et al.* [40,41] have made an extended series of observations of cavitation bubbles in the flow around axisymmetric bodies, including studies of the scaling of the phenomena. The observations at lower Reynolds numbers are exemplified by the photographs of bubble profiles in figure 12 and 13. In all cases the shape during the initial growth phase is that of a spherical cap, the bubble being separated from the wall by a thin layer of liquid of the same order of magnitude as the boundary

layer thickness. Later developments depend on the geometry of the headform and the Reynolds number. In some cases as the bubble enters the region of adverse pressure gradient, the exterior frontal surface is pushed inward, causing the profile of the bubble to appear wedge-like. Thus the collapse is initiated on the exterior frontal surface of the bubble, and this often leads to the bubble fissioning into forward and aft bubbles as seen in figure 12.

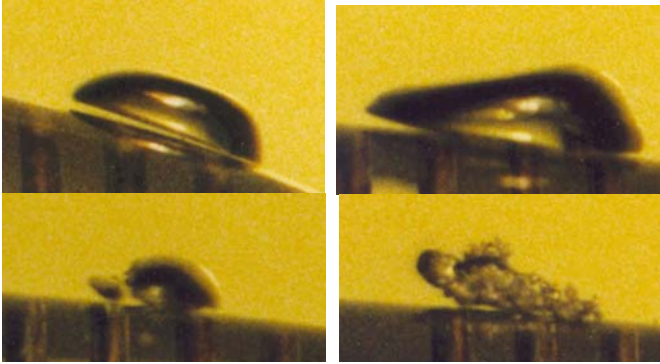


Figure 12. A series of photographs illustrating, in profile, the growth and collapse of a traveling cavitation bubble in a flow around a 5.08cm diameter headform at  $\sigma = 0.45$  and a speed of 9m/s. The sequence is top left, top right, bottom left, bottom right, the flow is from right to left. The lifesize width of each photograph is 0.73cm [39].

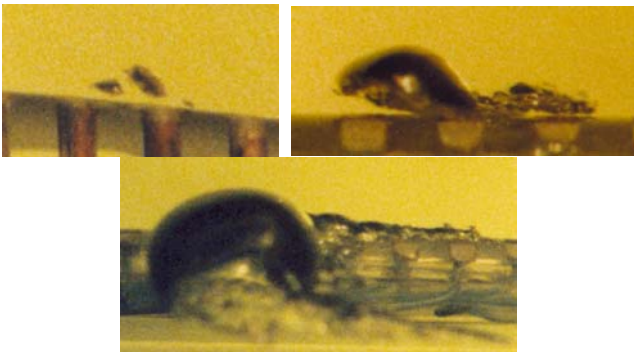


Figure 13. Examples of bubble fission (upper left), the instability of the liquid layer under a traveling cavitation bubble (upper right) and the attached tails (lower) [39] from experiments with a 5.08cm diameter ITTC headform at  $\sigma = 0.45$  and a speed of 8.7m/s. The flow is from right to left. The lifesize widths of the photographs are 0.63cm, 0.80cm and 1.64cm respectively.

At the same time, the bubble acquires significant spanwise vorticity through its interactions with the boundary layer during the growth phase. Consequently, as the collapse proceeds, this vorticity is concentrated and the bubble evolves into one (or two or possibly more) short cavitating vortices with spanwise axes. These vortex bubbles proceed to collapse and seem to rebound as a cloud of much smaller bubbles.

Ceccio and Brennen [39] (see also Kumar and Brennen [42]) conclude that the flow-induced fission prior to collapse can have a substantial effect on the noise produced.



Figure 14. Typical cavitation events from the scaling experiments of Kuhn de Chizelle *et al.* [41] showing transient bubble-induced patches, the left one occurring on a 50.8cm diameter Schiebe headform at  $\sigma = 0.605$  and a speed of 15m/s, the right one on a 25.4cm headform at  $\sigma = 0.53$  and a speed of 15 m/s. The flow is from right to left. The lifesize widths of the photographs are 6.3cm (left) and 7.6cm (right).

Two additional phenomena were observed. In some cases the layer of liquid underneath the bubble would become disrupted by some instability, creating a bubbly layer of fluid that subsequently gets left behind the main bubble (see figure 13). Second, it sometimes happened that when a bubble passed a point of laminar separation, it triggered the formation of local *attached cavitation* streaks at the lateral or spanwise extremities of the bubble, as seen in figure 13. Then, as the main bubble proceeds downstream, these *streaks* or *tails* of attached cavitation are stretched out behind the main bubble, the trailing ends of the tails being attached to the solid surface. Tests at much higher Reynolds numbers (Kuhn de Chizelle *et al.* [40,41]) revealed that these events with tails occurred more frequently and would initiate attached cavities over the entire wake of the bubble as seen in figure 14. Moreover, the attached cavitation would tend to remain for a longer period after the main bubble had disappeared. Eventually, at the highest Reynolds numbers tested, it appeared that the passage of a single bubble was sufficient to trigger a patch of attached cavitation (figure 14, right), that would persist for an extended period after the nucleus had long disappeared.

In summary, cavitation bubbles are substantially deformed and their dynamics and acoustics altered by the flow fields in which they occur. This necessarily changes the noise and damage produced by those cavitation events.

## 11. CAVITATION NOISE

The violent and catastrophic collapse of cavitation bubbles results in the production of noise that is a consequence of the momentary large pressures that are generated when the contents of the bubble are highly compressed. Consider the flow in the liquid caused by the unsteady volume,  $V(t)$ , of a growing or collapsing cavity. In the far field the flow will approach that of a



simple source/sink, and will therefore be associated with a radiated acoustic pressure,  $p_a(t)$ , given by

$$p_a = \frac{\rho_L}{4\pi R} \frac{d^2V}{dt^2}$$

where we denote the distance from the cavity center to the point of measurement by  $R$  (for a more thorough treatment see Dowling and Ffowcs Williams [43] and Blake [44]). Thus the noise pulse generated at bubble collapse occurs because of the very large and positive values of  $d^2V/dt^2$  when the bubble is close to its minimum size. It is conventional (see, for example, Blake [44]) to present the sound level using a root mean square pressure or *acoustic* pressure,  $p_s$ , defined by

$$p_s^2 = \overline{p_a^2} = \int_0^\infty G(f) df$$

and to represent the distribution over the frequency range,  $f$ , by the spectral density function,  $G(f)$ .

To the researcher or engineer, the crackling noise that accompanies cavitation is one of the most evident characteristics of the phenomenon. The onset of cavitation is often detected first by this noise rather than by visual observation of the bubbles. Moreover, for the practical engineer it is often the primary means of detecting cavitation in devices such as pumps and valves. Indeed, several empirical methods have been suggested that estimate the rate of material damage by measuring the noise generated (for example, Lush and Angell [45]).

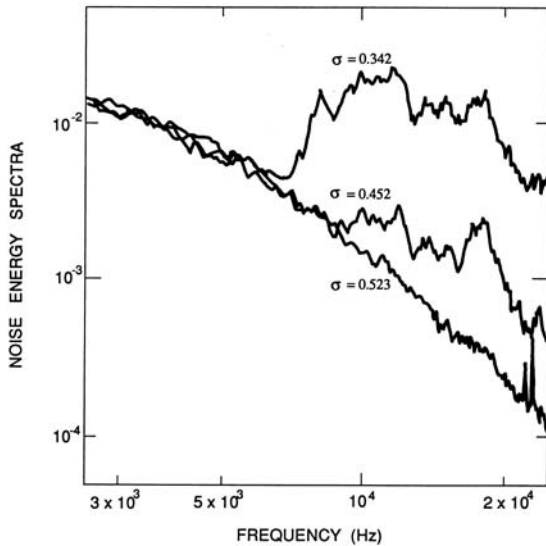


Figure 15. Acoustic power spectra from a model spool valve operating under noncavitating ( $\sigma=0.523$ ) and cavitating ( $\sigma=0.452$  and  $0.342$ ) conditions (from the investigation of Martin *et al.* [49]).

The noise due to cavitation in the orifice of a hydraulic control valve is typical, and spectra from such

an experiment are presented in figure 15. The lowest curve at  $\sigma=0.523$  represents the turbulent noise from the noncavitating flow. Below the incipient cavitation number (about 0.523 in this case) there is a dramatic increase in the noise level at frequencies of about 5kHz and above. The spectral peak between 5kHz and 10kHz corresponds closely to the expected natural frequencies of the nuclei present in the flow (see above). Most of the analytical approaches to cavitation noise build on knowledge of the dynamics of collapse of a single bubble. Fourier analyses of the radiated acoustic pressure due to a single bubble were first visualized by Rayleigh [46] and implemented by Mellen [47] and Fitzpatrick and Strasberg [48].

Since the volume of the bubble increases from near-zero to a finite value and then returns to near-zero, it follows that for frequencies less than the inverse of the time for this process, the Fourier transform of the volume is independent of frequency. Consequently  $d^2V/dt^2$  will be proportional to  $f^2$  and therefore  $G(f)$  is proportional to  $f^4$  [48]. This is the origin of the left-hand asymptote in figure 16.

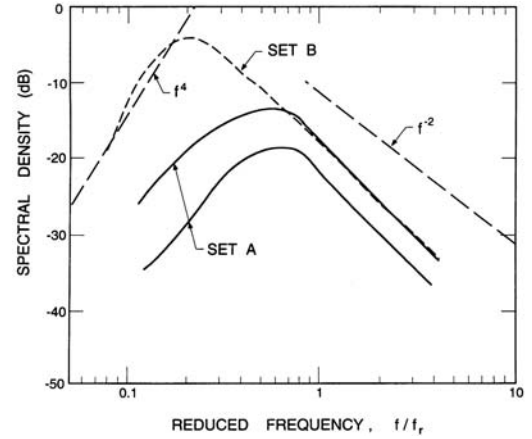


Figure 16. Acoustic power spectra of the noise from a cavitating jet. Shown are mean lines through two sets of data constructed by Blake and Sevik [51] from the data by Jorgensen [50]. Typical asymptotic behaviors are also indicated. The reference frequency,  $f_r$ , is  $(p_{\infty}/\rho_L d^2)^{1/2}$  where  $d$  is the jet diameter.

The behavior at intermediate frequencies has been the subject of more speculation and debate. Mellen [47] and others considered the typical equations governing the collapse of a spherical bubble in the absence of thermal effects and noncondensable gas and concluded that, since the velocity  $dR/dt$  is proportional to  $R^{-3/2}$ , it follows that  $R$  is proportional to  $t^{2/5}$ . Therefore the Fourier transform of  $d^2V/dt^2$  leads to the asymptotic behavior of  $G(f)$  proportional to  $f^{2/5}$ . The error in this analysis is the neglect of the noncondensable gas. When this is included and when the collapse is sufficiently advanced, the behavior is quite different. Moreover, the values of  $d^2V/dt^2$  are much larger during

this rebound phase, and therefore the frequency content of the rebound phase will dominate the spectrum. It is therefore not surprising that the  $f^{2/5}$  is not observed in practice. Rather, most of the experimental results seem to exhibit an intermediate frequency behavior like  $f^1$  or  $f^2$ . Jorgensen [50] measured the noise from submerged, cavitating jets and found a behavior like  $f^2$  at the higher frequencies; however, most of the experimental data for cavitating bodies or hydrofoils exhibit a weaker decay. The data by Arakeri and Shangumanathan [54] from cavitating headform experiments show a very consistent  $f^1$  trend over almost the entire frequency range, and very similar results have been obtained by Ceccio and Brennen [39].

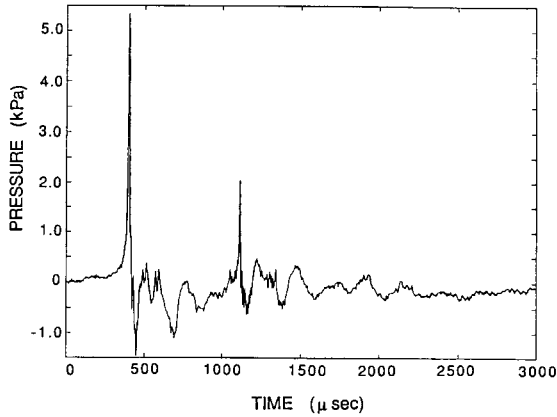


Figure 17. A typical acoustic signal from a single collapsing bubble [39].

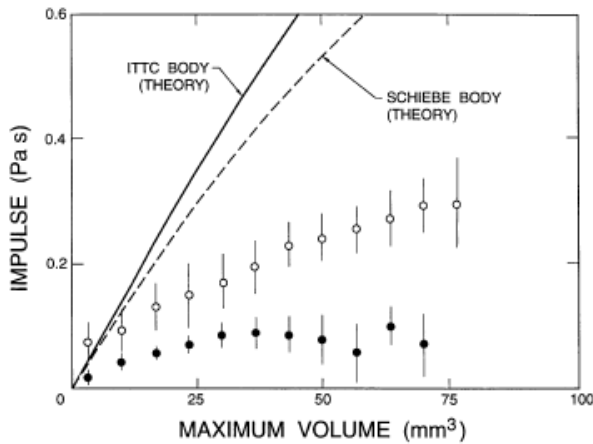


Figure 18. Comparison of the acoustic impulse,  $I$ , produced by the collapse of a single cavitation bubble on two axisymmetric headforms as a function of the maximum volume prior to collapse. Open symbols: Schiebe body; closed symbols: ITTC body; vertical lines indicate one standard deviation. Also shown are the corresponding results from the solution of the Rayleigh-Plesset equation [39].

Ceccio and Brennen [39] recorded the noise from individual cavitation bubbles in a flow and a typical

acoustic signal from their experiments is reproduced in figure 17. The large positive pulse at about 450  $\mu$ s corresponds to the first collapse of the bubble. This first pulse in figure 17 is followed by some facility-dependent oscillations and by a second pulse at about 1100  $\mu$ s. This corresponds to the second collapse that follows the rebound from the first collapse.

A good measure of the magnitude of the collapse pulse is the acoustic impulse,  $I$ , defined as the area under the pulse or

$$I = \int_{t_1}^{t_2} p_a dt$$

where  $t_1$  and  $t_2$  are times before and after the pulse at which  $p_a$  is zero. For later purposes we also define a dimensionless impulse,  $I^*$ , as

$$I^* = 4\pi IR / \rho_L U \ell^2$$

where  $U$  and  $\ell$  are the reference velocity and length in the flow. The average acoustic impulses for individual bubble collapses on two axisymmetric headforms (ITTC and Schiebe bodies) are compared in figure 18 with impulses predicted from integration of the Rayleigh-Plesset equation. Since these theoretical calculations assume that the bubble remains spherical, the discrepancy between the theory and the experiments is not too surprising. Indeed one interpretation of figure 18 is that the theory can provide an order of magnitude estimate and an upper bound on the noise produced by a single bubble. In actuality, the departure from sphericity produces a less focused collapse and therefore less noise.

The next step is to consider the synthesis of cavitation noise from the noise produced by individual cavitation bubbles or events. If the impulse produced by each event is denoted by  $I$  and the number of events per unit time is denoted by  $n^*$ , the sound pressure level,  $p_s$ , will be given by  $p_s = I n^*$ . Consider the scaling of cavitation noise that is implicit in this construct. Both the experimental results and the analysis based on the Rayleigh-Plesset equation indicate that the nondimensional impulse,  $I^*$ , produced by a single cavitation event is strongly correlated with the maximum volume of the bubble prior to collapse and is almost independent of the other flow parameters. It follows [9] that

$$I^* = \frac{1}{U \ell^2} \left\{ \left( \frac{dV}{dt} \right)_{t_2} - \left( \frac{dV}{dt} \right)_{t_1} \right\}$$

and the values of  $dV/dt$  at the moments  $t=t_1, t_2$  when  $d^2V/dt^2=0$  may be obtained from the Rayleigh-Plesset equation. If the bubble radius at the time  $t_1$  is denoted by  $R_x$  and the coefficient of pressure in the liquid at that moment is denoted by  $C_{px}$ , then

$$I^* \approx 8\pi \left( \frac{R_x}{\ell} \right)^2 (C_{px} - \sigma)^{\frac{1}{2}}$$

Numerical integrations of the Rayleigh-Plesset equation for a range of typical circumstances yield  $R_x/R_m \sim 0.62$  where  $R_m$  is the maximum volumetric radius and that

$$(C_{px} - \sigma) \propto R_m/\ell$$

(in these calculations  $\ell$  was the headform radius) so that

$$I^* \approx \beta \left( \frac{R_m}{\ell} \right)^{\frac{5}{2}}$$

The aforementioned integrations of the Rayleigh-Plesset equation yield the factor of proportionality,  $\beta$ , of about 35. On the other hand the experimental data on  $I^*$  [39, 40, 41] suggest a maximum value of  $\beta$  of about 4. We note that a quite similar relation between  $I^*$  and  $R_m/\ell$  emerges from the analysis by Esipov and Naugol'nykh [52] of the compressive sound wave generated by the collapse of a gas bubble in a compressible liquid.

Consequently, the evaluation of the impulse from a single event is completed by an estimate of  $R_m$  such as that presented earlier. Since that estimate has  $R_m$  independent of  $U$  for a given cavitation number, it follows that  $I$  is linear with  $U$ . The event rate,  $n^*$ , can be considerably more complicated to evaluate than might at first be thought but begins with an evaluation of all the nuclei of concentration  $N$  (number per unit volume) flowing through an appropriate streamtube of cross-sectional area,  $A_N$ , with velocity,  $U_{oo}$ , so that  $n^* = NAU_{oo}$ . Then

$$PS \approx \frac{\beta}{3} \rho_L U_{\infty}^2 A_N N R_H^2 (-\sigma - C_{pmin})^{\frac{5}{2}} / R$$

where we have omitted some of the constants of order unity. For the relatively simple flows considered here, this equation yields a sound pressure level that scales with  $U_{oo}^2$  and with  $\ell^4$  because  $A_N$  is proportional to  $\ell^2$ . This scaling with velocity does correspond roughly to that which has been observed in some experiments on traveling bubble cavitation, for example, those of Blake, Wolpert, and Geib [53] and Arakeri and Shangumanathan [54]. The former observe that  $p_s$  is proportional to  $U_{oo}^m$  where  $m = 1.5$  to  $2$ . Different scaling laws will apply when the cavitation is generated by turbulent fluctuations such as in a turbulent jet (see, for example, Franklin and McMillan [55]). Then the typical tension experienced by a nucleus as it moves along a disturbed path in a turbulent flow is very much more difficult to estimate. Consequently, the models for the sound pressure due to cavitation in a turbulent flow and the scaling of that sound with velocity are less well understood.

## 12. CLOUD CAVITATION

In many cavitating liquid flows, when the number and concentration of the bubbles exceeds some critical level, the flow becomes unsteady and large clouds of cavitating bubbles are periodically formed and then collapse when convected into regions of higher pressure. This phenomenon is known as cloud cavitation and when it occurs it is almost always associated with a substantial increase in the cavitation noise and damage. We note that sometimes the clouds are large as in breaking waves and large shed vortices (Figure 19). But they can also be small, for example due to fission of a single collapsed cavitation bubble (Figure 8).



Figure 19. Examples of bubble clouds. Left: clouds formed downstream of an artificial heart valve closure (Rambod *et al.* [69]). Right: clouds formed in the wake of an oscillating hydrofoil

The highly destructive consequences of cloud cavitation have been known for a long time and have been documented, for example, by Knapp [56], Bark and van Berlekom [57] and Soyama *et al.* [58]. The generation of these cavitation clouds may occur naturally as a result of the shedding of bubble-filled vortices, or it may be the response to a periodic disturbance imposed on the flow. Common examples of imposed fluctuations are the interaction between rotor and stator blades in a pump or turbine, the interaction between a ship's propeller and the non-uniform wake created by the hull and the periodic opening and closing of a heart valve. As a result numerous investigators (for example, Wade and Acosta [59], Bark and van Berlekom [57], Shen and Peterson [60,61], Bark [62], Franc and Michel [63], Hart *et al.* [64], Kubota *et al.* [65], Le *et al.* [66], de Lange *et al.* [67]) have studied the complicated flow patterns involved in the production and collapse of cloud cavitation, most of them examining a single hydrofoil. The radiated noise produced is characterized by pressure pulses of very short duration and large magnitude. These pressure pulses have been measured by Bark [62], Bark and van Berlekom [57], Le *et al.* [66], Shen and Peterson [60,61] and McKenney and Brennen [68].

Here we briefly review analyses of cloud cavitation in simplified geometries that allow us to anticipate the behavior of clouds of cavitation bubbles and the parameters that influence that behavior. These simpler geometries allow some anticipation of the role of cloud cavitation in more complicated flows such as those in cavitating pumps.

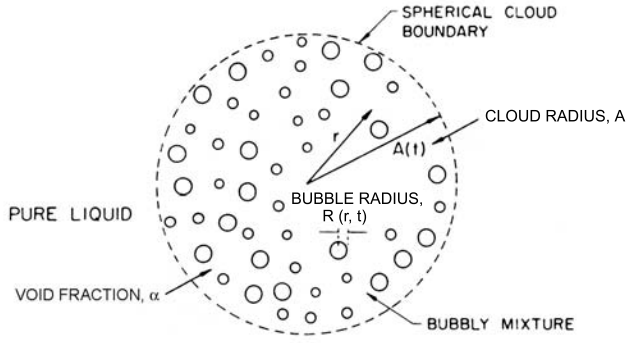


Figure 20. Schematic of a spherical cloud of cavitation bubbles [71,72].

Though the first analysis that indicated how bubbles might behave collectively was conducted by van Wijngaarden [70] on a plane layer of bubbles next to a wall, it is more convenient to focus attention on a finite spherical cloud surrounded by pure liquid and to briefly review the dynamics and acoustics of such a cloud. We begin with the simplified case shown in figure 20 in which all the bubbles in the cloud have the same equilibrium size,  $R_0$ , and are uniformly distributed within the cloud. Thus the population as represented by the initial equilibrium void fraction,  $\alpha_0$ , is uniform within the cloud. Radial position within the cloud is denoted by  $r$  and the initial radius of the cloud by  $A_0$ .

d'Agostino and Brennen [71,72] showed that a linearized dynamics analysis of such a cloud reveals that it has its own, infinite set of natural frequencies denoted by  $\omega_n$  and given by

$$\omega_n = \omega_N \left[ 1 + \frac{4}{3\pi^2(2n-1)^2} \frac{A_0^2}{R_0^2} \frac{\alpha_0}{1-\alpha_0} \right]^{-\frac{1}{2}}$$

for  $n = 1, 2, 3, \dots$  and where  $\omega_N$  is the previously quoted natural frequency of an individual bubble oscillating alone in an infinite liquid. The above is an infinite series of frequencies of which  $\omega_1$  is the lowest. The higher frequencies approach  $\omega_N$  as  $n$  tends to infinity.

As expected these natural frequencies correspond to modes with more and more nodes as  $n$  increases (see Brennen [9]). Note that the lowest natural frequency,  $\omega_1$ , is given by

$$\omega_1 = \omega_N \left[ 1 + \frac{4}{3\pi^2} \frac{A_0^2}{R_0^2} \frac{\alpha_0}{1-\alpha_0} \right]^{-\frac{1}{2}}$$

Note also that this can be much smaller than  $\omega_N$  if the initial void fraction,  $\alpha_0$ , is much larger than the square of the ratio of bubble size to cloud size,  $\alpha_0 \gg R_0^2/A_0^2$ . If the reverse is the case ( $\alpha_0 \ll R_0^2/A_0^2$ ) all the natural frequencies of the cloud are contained in a small range just below  $\omega_N$ . This defines a special parameter,  $\beta = \alpha_0 A_0^2/R_0^2$ , that governs the cloud interaction effects and that is termed the "Cloud Interaction Parameter".

If  $\beta \ll 1$  there is relatively little bubble interaction effect and all the bubbles oscillate at close to the frequency,  $\omega_N$ , as if each were surrounded by nothing but liquid. On the other hand when  $\beta > 1$  the cloud has natural frequencies much less than  $\omega_N$  and there are strong interaction effects between the bubbles in the cloud.

Note that in various applications the magnitude of  $\beta$  could take a wide range of values from much less than unity to much greater than unity. It will be small in small clouds with a few large bubbles and a low void fraction but could be large in large clouds of small bubbles with higher void fraction.

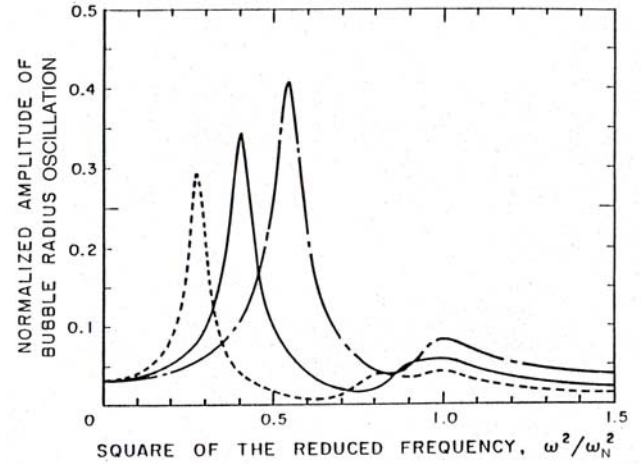


Figure 21. The amplitude of the bubble radius oscillation at the cloud surface as a function of frequency for damped oscillations at three values of  $\beta = 0.8$  (solid line),  $\beta = 0.4$  (dot-dash line), and  $\beta = 1.65$  (dashed line). From d'Agostino and Brennen [72].

d'Agostino and Brennen [71,72] examined the forced linearized response of a cloud to oscillations in the pressure in the liquid far from the bubble. When a reasonable estimate of the damping is included, the attenuation of the higher frequencies is much greater so the dominant peak in the response occurs at the lowest natural frequency of the cloud, namely  $\omega_1$ . The response at the bubble natural frequency,  $\omega_N$ , becomes much less significant. This conclusion and the effect of varying the cloud interaction parameter,  $\beta$ , is shown in figure 21, where the amplitude of bubble radius oscillation at the cloud surface is presented as a function of frequency. Note that increasing  $\beta$  causes a reduction in both the amplitude and frequency of the dominant response at the lowest natural frequency of the cloud.

The above results are all from linear analyses and we conclude our discussion of cloud effects by describing calculations of the large amplitude non-linear analyses. If a spherical cloud is subjected to an episode of sufficiently low pressure it will cavitate, in other words the bubbles will grow explosively to many times their original size. Subsequently, if the pressure far from the



cloud increases again (as, for example, when the cloud is convected out of the region of low pressure) the bubbles will collapse violently. We previously described the response of a single bubble to such a pressure episode; the response of a cloud of bubbles is more complex.

A valuable perspective on the subject was that introduced by Morch [73,74,75] and Hanson, Kedrinskii and Morch [76]. They suggested that the collapse of a cloud of bubbles involves the formation and inward propagation of a shock wave and that the geometric focusing of this shock at the center of cloud creates the enhancement of the noise and damage potential associated with cloud collapse. Wang and Brennen [77,78] and Reisman et al. [79] employed the use of continuity and momentum equations coupled to the Rayleigh-Plesset equation in order to model the two-phase flow within the cloud. Here we briefly review their numerical calculations that detailed the dynamics of a spherical cloud of cavitating bubbles..

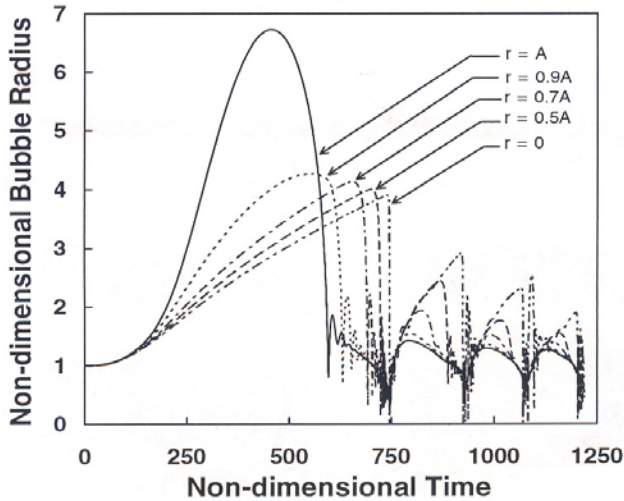


Figure 22. Typical time history of the bubble size at six different Lagrangian positions in a spherical cloud in response to an episode of reduced pressure in the surrounding liquid (between  $t=0$  and  $t=250$ ). This figure is for the parameter  $\beta$  much greater than unity [77,78].

It transpires that the response of a cloud to an episode of reduced pressure in the surrounding liquid is quite different depending on the magnitude of  $\beta$ . When  $\beta$  is much greater than unity the typical cloud response to an episode of reduced pressure is shown in figure 22 (upper). Note that the bubbles on the surface of the cloud grow more rapidly than those in the interior which are effectively shielded from the reduced pressure in the surrounding liquid. More importantly the bubbles on the surface collapse first and a collapse front propagates inward from the cloud surface developing into a substantial shock wave. Due to geometric focusing this shock wave strengthens as the shock proceeds inwards

and creates a very large pressure pulse when it reached the center of the cloud.

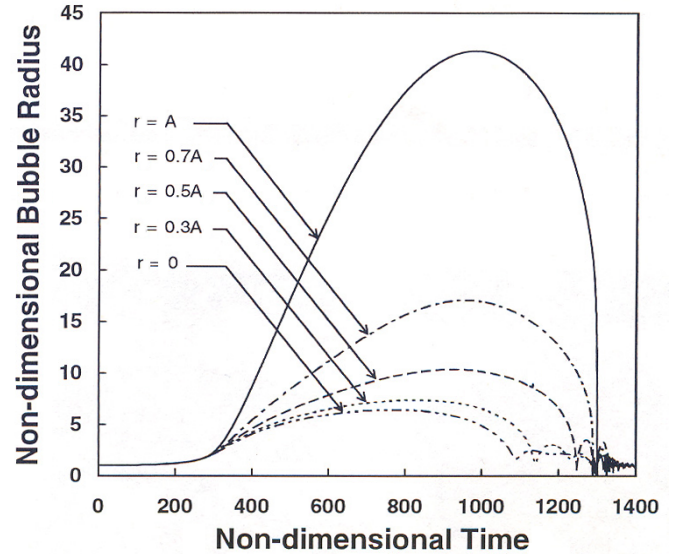


Figure 23. As Figure 22 but for  $\beta$  order unity or less [77,78].

On the other hand when  $\beta$  is small, the response of the cloud is quite different as shown in figure 23. Then the bubbles at the center of the cloud collapse first, resulting in an outgoing collapse front that weakens geometrically resulting in a quite different and much more benign dynamic.

While real bubble clouds are often far from spherical the potential for similar shielding and focussing effects still clearly exist.

### 13. CONCLUDING COMMENTS

This condensed review is an attempt to summarize at least some of the fundamental analyses and observations pertaining to cavitating flow. Of necessity we have omitted a huge literature of experimental observations and we have not covered important new results using modern computational techniques as well as research methodologies that use parallel experimental observations and computations of these high-speed events. Many challenges remain; for example the desire to accurately compute these complex, high-speed multiphase flows, an objective made doubly difficult by the multiple time and space scales of the flows.

### ACKNOWLEDGEMENTS

My sincerest thanks to all graduate students and post-doctoral fellows who contributed to the results described herein. I am also appreciative of the support from the Office of Naval Research who sponsored a good fraction of the research described.

## REFERENCES

- [1] Brennen, C.E. 2005. Fundamentals of multiphase flow. Cambridge University Press.
- [2] Peterson, F.B., Danel, F., Keller, A.P., and Lecoffre, Y. 1975. Comparative measurements of bubble and particulate spectra by three optical methods. Proc. 14th Int. Towing Tank Conf.
- [3] Gates, E.M. and Bacon, J. 1978. Determination of cavitation nuclei distribution by holography. J. Ship Res., 22, No. 1, 29-31.
- [4] Katz, J. 1978. Determination of solid nuclei and bubble distributions in water by holography. Calif. Inst. of Tech., Eng. and Appl. Sci. Div. Rep. No. 183-3.
- [5] O'Hern, T.J., Katz, J., and Acosta, A.J. 1985. Holographic measurements of cavitation nuclei in the sea. Proc. ASME Cavitation and Multiphase Flow Forum, 39-42.
- [6] Knapp, R.T., Daily, J.W., and Hammitt, F.G. 1970. Cavitation. McGraw-Hill, New York.
- [7] Acosta, A.J. and Parkin, B.R. 1975. Cavitation inception--a selective review. J. Ship Res., 19, 193-205.
- [8] Arakeri, V.H. 1979. Cavitation inception. Proc. Indian Acad. Sci., C2, Part 2, 149-177.
- [9] Brennen, C.E. 1995. Cavitation and bubble dynamics. Oxford University Press.
- [10] Knapp, R.T., Daily, J.W., and Hammitt, F.G. 1970. Cavitation. McGraw-Hill, New York.
- [11] Young, F.R. 1989. Cavitation. McGraw-Hill Book Company.
- [12] Herring, C. 1941. The theory of the pulsations of the gas bubbles produced by an underwater explosion. US Nat. Defence Res. Comm. Report.
- [13] Gilmore, F.R. 1952. The collapse and growth of a spherical bubble in a viscous compressible liquid. Calif. Inst. of Tech. Hydrodynamics Lab. Rep. No. 26-4.
- [12] Prosperetti, A. and Lezzi, A. 1986. Bubble dynamics in a compressible liquid. Part 1. First-order theory.
- [13] Keller, J.B. and Kolodner, I.I. 1956. Damping of underwater explosion bubble oscillations. J. Appl. Phys., 27, 1152-1161.
- [14] Hickling, R. and Plesset, M.S. 1964. Collapse and rebound of a spherical bubble in water. Phys. Fluids, 7, 7-14.
- [15] Ivany, R.D. and Hammitt, F.G. 1965. Cavitation bubble collapse in viscous, compressible liquids - numerical analysis. ASME J. Basic Eng., 87, 977-985.
- [16] Tomita, Y. and Shima, A. 1977. On the behaviour of a spherical bubble and the impulse pressure in a viscous compressible liquid. Bull. JSME, 20, 1453-1460.
- [17] Fujikawa, S. and Akamatsu, T. 1980. Effects of the non-equilibrium condensation of vapour on the pressure wave produced by the collapse of a bubble in a liquid. J. Fluid Mech., 97, 481-512.
- [18] Birkhoff, G. 1954. Note on Taylor instability. Quart. Appl. Math., 12, 306-309.
- [19] Plesset, M.S. and Mitchell, T.P. 1956. On the stability of the spherical shape of a vapor cavity in a liquid. Quart. Appl. Math., 13, No. 4, 419-430.
- [20] Naude, C.F. and Ellis, A.T. 1961. On the mechanism of cavitation damage by non-hemispherical cavities in contact with a solid boundary. ASME. J. Basic Eng., 83, 648-656.
- [21] Benjamin, T.B. and Ellis, A.T. 1966. The collapse of cavitation bubbles and the pressures thereby produced against solid boundaries. Phil. Trans. Roy. Soc., London, Ser. A, 260, 221-240.
- [22] Tomita, Y. and Shima, A. 1990. High-speed photographic observations of laser-induced cavitation bubbles in water. Acustica, 71, No. 3, 161-171.
- [23] Lauterborn, W. and Bolle, H. 1975. Experimental investigations of cavitation bubble collapse in the neighborhood of a solid boundary. J. Fluid Mech., 72, 391-399.
- [24] Plesset, M.S. and Chapman, R.B. 1971. Collapse of an initially spherical vapor cavity in the neighborhood of a solid boundary. J. Fluid Mech., 47, 283-290.
- [25] Plesset, M.S. and Prosperetti, A. 1977. Bubble dynamics and cavitation. Ann.Rev. Fluid Mech., 9, 145-185.
- [26] Chahine, G.L. (1977). Interaction between an oscillating bubble and a free surface. ASME J. Fluids Eng., 99, 709-716.
- [27] Gibson, D.C. and Blake, J.R. (1982). The growth and collapse of bubbles near deformable surfaces. Appl. Sci. Res., 38, 215-224.
- [28] Chahine, G.L. and Duraiswami, R. (1992). Dynamical interactions in a multibubble cloud. ASME J. Fluids Eng., 114, 680-686.
- [29] Frost, D. and Sturtevant, B. 1986. Effects of ambient pressure on the instability of a liquid boiling explosively at the superheat limit. ASME J. Heat Transfer, 108, 418--424.
- [30] Brennen, C.E. (2002). Fission of collapsing cavitation bubbles. J. Fluid Mech., 472, 153-166.
- [31] ASTM. 1967. Erosion by cavitation or impingement. Amer. Soc. for Testing and Materials, ASTM STP408
- [32] Thiruvengadam, A. 1967. The concept of erosion strength. In Erosion by cavitation or impingement. Am. Soc. Testing Mats. STP 408, 22-35.
- [33] Thiruvengadam, A. 1974. Handbook of cavitation erosion. Tech. Rep. 7301-1, Hydronautics, Inc., Laurel, Md.
- [34] Shima, A., Takayama, K., Tomita, Y., and Ohsawa, N. 1983. Mechanism of impact pressure generation from spark-generated bubble collapse near a wall. AIAA J., 21, 55-59.
- [35] Kimoto, H. 1987. An experimental evaluation of the effects of a water microjet and a shock wave by a local pressure sensor. Int. ASME Symp. on Cavitation Res. Facilities and Techniques, FED 57, 217-224.
- [36] Knapp, R.T. and Hollander, A. 1948. Laboratory investigations of the mechanism of cavitation. Trans. ASME, 70, 419-435.
- [37] Plesset, M.S. 1949. The dynamics of cavitation bubbles. ASME J. Appl. Mech., 16, 228-231.
- [38] Parkin, B.R. 1952. Scale effects in cavitating flow. Ph.D. Thesis, Calif. Inst. Of Tech.

- [39] Ceccio, S.L. and Brennen, C.E. 1991. Observations of the dynamics and acoustics of travelling bubble cavitation. *J. Fluid Mech.*, 233, 633-660.
- [40] Kuhn de Chizelle, Y., Ceccio, S.L., Brennen, C.E., and Gowing, S. 1992a. Scaling experiments on the dynamics and acoustics of travelling bubble cavitation. *Proc. 3rd I. Mech. E. Int. Conf. on Cavitation*, Cambridge, England, 165-170.
- [41] Kuhn de Chizelle, Y., Ceccio, S.L., Brennen, C.E., and Shen, Y. 1992b. Cavitation scaling experiments with headforms: bubble acoustics. *Proc. 19<sup>th</sup> ONR Symp. on Naval Hydrodynamics*, 72-84.
- [42] Kumar, S. and Brennen, C.E. 1993. A study of pressure pulses generated by travelling bubble cavitation. *J. Fluid Mech.*, 255, 541-564.
- [43] Dowling, A.P. and Ffowcs Williams, J.E. 1983. *Sound and sources of sound*. Ellis Horwood Ltd. and John Wiley and Sons.
- [44] Blake, W.K. 1986b. *Mechanics of flow-induced sound and vibration*. Academic Press.
- [45] Lush, P.A. and Angell, B. 1984. Correlation of cavitation erosion and sound pressure level. *ASME. J. Fluids Eng.*, 106, 347-351.
- [46] Rayleigh, Lord (Strutt, J.W.). 1917. On the pressure developed in a liquid during the collapse of a spherical cavity. *Phil. Mag.*, 34, 94-98.
- [47] Mellen, R.H. 1954. Ultrasonic spectrum of cavitation noise in water. *J. Acoust. Soc. Am.*, 26, 356-360.
- [48] Fitzpatrick, H.M. and Strasberg, M. 1956. Hydrodynamic sources of sound. *Proc. First ONR Symp. on Naval Hydrodynamics*, 241-280.
- [49] Martin, C.S., Medlarz, H., Wiggert, D.C., and Brennen, C. 1981. Cavitation inception in spool valves. *ASME. J. Fluids Eng.*, 103, 564-576.
- [50] Jorgensen, D.W. 1961. Noise from cavitating submerged jets. *J. Acoust. Soc. Am.*, 33, 1334-1338.
- [51] Blake, W.K. and Sevik, M.M. 1982. Recent developments in cavitation noise research. *Proc. ASME Int. Symp. on Cavitation Noise*, 1-10.
- [52] Esipov, I.B. and Naugol'nykh, K.A. 1973. Collapse of a bubble in a compressible liquid. *Akust. Zh.*, 19, 285-288.
- [53] Blake, W.K., Wolpert, M.J. and Geib, F.E. 1977. Cavitation noise and inception as influenced by boundary-layer development on a hydrofoil. *J. Fluid Mech.*, 80, 617-640.
- [54] Arakeri, V.H. and Shangumanathan, V. 1985. On the evidence for the effect of bubble interference on cavitation noise. *J. Fluid Mech.*, 159, 131-150.
- [55] Franklin, R.E. and McMillan, J. 1984. Noise generation in cavitating flows, the submerged jet. *ASME J. Fluids Eng.*, 106, 336-341.
- [56] Knapp, R.T. 1955. Recent investigations of the mechanics of cavitation and cavitation damage. *Trans. ASME*, 77, 1045-1054.
- [57] Bark, G., and Berlekom, W.B. 1978. Experimental Investigations of Cavitation Noise. *Proc. 12th ONR Symp. on Naval Hydrodynamics*, 470-493.
- [58] Soyama, H., Kato, H., and Oba, R. 1992. Cavitation Observations of Severely Erosive Vortex Cavitation Arising in a Centrifugal Pump. *Proc. Third I.Mech.E. Int. Conf. on Cavitation*, 103-110.
- [59] Wade, R.B. and Acosta, A.J. 1966. Experimental Observations on the Flow Past a Plano-Convex Hydrofoil. *ASME J. Basic Eng.*, 88, 273-283.
- [60] Shen, Y., and Peterson, F.B. 1978. Unsteady Cavitation on an Oscillating Hydrofoil. *Proc. 12th ONR Symposium on Naval Hydrodynamics*, 362-384.
- [61] Shen, Y., and Peterson, F.B. 1980. The Influence of Hydrofoil Oscillation on Boundary Layer Transition and Cavitation Noise. *Proc. 13th ONR Symposium on Naval Hydrodynamics*, 221-241.
- [62] Bark, G. 1985. Developments of Distortions in Sheet Cavitation on Hydrofoils. *Proc. ASME Int. Symp. on Jets and Cavities*, 470-493.
- [63] Franc, J.P., and Michel, J.M. 1988. Unsteady Attached Cavitation on an Oscillating Hydrofoil. *J. Fluid Mech.*, 193, 171-189.
- [64] Hart, D.P., Brennen, C.E. and Acosta, A.J. 1990. Observations of cavitation on a three dimensional oscillating hydrofoil. *ASME Cavitation and Multiphase Flow Forum*, FED-98, 49-52.
- [65] Kubota, A., Kato, H., Yamaguchi, H. and Maeda, M. 1989. Unsteady structure measurement of cloud cavitation on a foil section using conditional sampling. *ASME J. Fluids Eng.*, 111, 204-210.
- [66] Le, Q., Franc, J. M. and Michel, J. M. 1993. Partial cavities: global behaviour and mean pressure distribution. *ASME J. Fluids Eng.*, 115, 243-248.
- [67] de Lange, D.F., de Bruin, G.J. and van Wijngaarden, L. 1994. On the mechanism of cloud cavitation - experiment and modeling. *Proc. 2nd Int. Symp. on Cavitation*, Tokyo, 45-50.
- [68] McKenney, E.A. and Brennen, C.E. 1994. On the dynamics and acoustics of cloud cavitation on an oscillating hydrofoil. *Proc. ASME Symp. on Cavitation and Gas-Liquid Flows in Fluid Machinery and Devices*, FED-190, 195-202.
- [69] Rambod, E., Beizaie, M., Shusser, M., Milo, S. and Gharib, M. 1999. A physical model describing the mechanism for formation of gas microbubbles in patients with mitral mechanical heart valves. *Ann. Biomed. Eng.*, 27, 774-792.
- [70] van Wijngaarden, L. 1964. On the collective collapse of a large number of gas bubbles in water. *Proc. 11th Int. Conf. Appl. Mech.*, Springer-Verlag, Berlin, 854-861.
- [71] d'Agostino, L. and Brennen, C.E. 1983. On the acoustical dynamics of bubble clouds. *ASME Cavitation and Multiphase Flow Forum*, 72-75.
- [72] d'Agostino, L. and Brennen, C.E. 1989. Linearized dynamics of spherical bubble clouds. *J. Fluid Mech.*, 199, 155-176.
- [73] Morch, K.A. 1980. On the collapse of cavity cluster in flow cavitation. *Proc. First Int. Conf. on Cavitation and*

Inhomogenities in Underwater Acoustics, Springer Series in Electrophysics, 4, 95--100.

[74] Morch, K.A. 1981. Cavity cluster dynamics and cavitation erosion. Proc. ASME Cavitation and Polyphase Flow Forum, 1--10.

[75] Morch, K.A. 1982. Energy considerations on the collapse of cavity cluster. Appl. Sci. Res., 38, 313.

[76] Hanson, I., Kedrinskii, V.K. and Morch, K.A. 1981. On the dynamics of cavity clusters. J. Appl. Phys., 15, 1725--1734.

[77] Wang, Y.-C. and Brennen, C.E. 1995a. The noise generated by the collapse of a cloud of cavitation bubbles. Proc. ASME/JSME Symp. on Cavitation and Gas-Liquid Flow in Fluid Machinery and Devices, FED-226, 17--29.

[78] Wang, Y.-C. and Brennen, C.E. 1995b. Shock wave and noise in the collapse of a cloud of cavitation bubbles. Proc. 20th Int. Symp. on Shock Waves, 1213--1218.

[79] Reisman, G.E., Wang, Y.-C. and Brennen, C.E. 1998. Observations of shock waves in cloud cavitation. J. Fluid Mech., 355, 255--283.



